Morphological and chemical evidence for cyclic bone growth in a fossil hyaena†

Jennifer Anné, *[ab] Roy A. Wogelius,[ac] Nicholas P. Edwards,[ad] Arjen van Veelen,[ce] Michael Buckley,[a] William I. Sellers,[a] Uwe Bergmann,[f] Dimosthenis Sokaras,[d] Roberto Alonso-Mori,[d] Virginia L. Harvey,[a] Victoria M. Egerton[ab] and Phillip L. Manning[ab]

Trace element inventories are known to correlate with specific histological structures in bone, reflecting organismal physiology and life histories. By studying trace elements in fossilised bone, particularly in individuals with cyclic bone growth (alternating fast/slow bone deposition), we can improve our understanding of the physiology of extinct organisms. In this study we present the first direct comparison between optical histology (bone tissue identification) and synchrotron-based chemical mapping, quantification, and characterisation of trace elements (biochemistry) within cyclic growth tissues, in this case within bones of a cave hyaena (*Crocuta crocuta spelaea*). Results show distributions of zinc, an element strongly associated with active ossification and bone growth, correlating with (1) fast-growing tissue of zonal bone (cyclic growth) in an extinct hyaena and (2) secondary osteons (remodelling) in both extant and extinct hyaena. Concentrations and coordination chemistry of zinc within the fossil sample are comparable to those seen in extant bone suggesting that zinc is endogenous to the sample and that the chemistry of bone growth has been preserved for 40 ka. These results demonstrate that the study of trace elements as part of the histochemistry has wide utility for reconstructing growth, diet and other lifestyle factors in archaeological and fossil bone.

Introduction

The physiology and life history of vertebrates are reflected in the microstructure of their skeletons (histology). As most vertebrate remains are preserved solely as bones, these tissues can provide key information on the physiology of extinct organisms such as metabolism and biological cycles. It is through such studies that we are able to identify key changes in vertebrate physiology though time, highlighting the adaptability of vertebrates to new and/or changing environments.

One of the physiological processes recorded in bone is the growth rate throughout an individual's life, which can be characterised by cyclic growth. These are fluctuations in bone depositional rates recognised in histological sections as alternating bands, known as zonal tissues, which are indicative of slow and fast growth.[1–7] It has previously been presumed that zonal bone is a characteristic of poikilothermic (slow metabolism) physiology due to the association of homeotherms (fast metabolism) with uninterrupted high rates of growth until maturity.[2–4] This paradigm has recently been challenged with the identification of zonal bone in a wide range of fossil and extant mammalian and avian groups.[1–3,5–7] However, it is still unclear how widespread zonal bone is within vertebrates, and thus what controls are placed on the plasticity of bone growth. Zonal bone formation has been attributed to changes in food/water sources, changes in temperature/thermoregulation, migration, sexual maturity and reproduction.[2,4,6] As stress affects the biochemical signalling that controls the rate of bone deposition, it is likely that mediating factors behind such signalling, such as compositional differences, may also be preserved within zonal tissues.

In addition to changes in bone microstructure, changes in bone physiology can also be characterised through trace element inventories. Previous studies have shown that the key trace elements for bone physiology (most notably Cu, Zn and Sr) can be mapped within discrete histological features, which correlate to specific physiological processes such as active

[a]*University of Manchester, School of Earth and Environmental Sciences, Interdisciplinary Centre for Ancient Life, Manchester M13 9PL, UK. E-mail: janne@childrensmuseum.org*

[b]*The Children's Museum of Indianapolis, Indianapolis, IN, 46208, USA*

[c]*University of Manchester, School of Earth and Environmental Sciences, Williamson Research Centre for Molecular Environmental Science, Manchester M13 9PL, UK*

[d]*SLAC National Accelerator Laboratory, Menlo Park, CA, 94025, USA*

[e]*University of Southampton, Faculty of Engineering and the Environment, Southampton, SO17 1BJ, UK*

[f]*Stanford PULSE Institute, SLAC National Accelerator Laboratory, Menlo Park, CA 95025, USA*

† Electronic supplementary information (ESI) available. See DOI: 10.1039/c8ja00314a

ossification and remodelling.[8–15] The distinct association with trace metals is a function of low concentrations (ppm) of organometallic compounds necessary for bone development, health and function, and the catalysis of enzymatic processes. Thus trace element inventories in bone can indicate the activity of physiological processes such as changes in bone growth. As zonal bone represents alternating fast (zones) and slow (annuli) depositional tissues, the trace element inventories associated with bone growth should reflect these changes in depositional rates. Therefore, by comparing differences in chemical inventories between the two tissue types, we can gain a better understanding of the physiological processes that control the switch between the two depositional rates.

Until recently, investigations into such chemical/histological correlations have not been attempted as commonly available techniques are unable to resolve the discrete variations (ppm levels) in chemistry at the necessary resolution (micron) and scale (decimetre). However, recent work using synchrotron-based X-ray fluorescence (XRF) has demonstrated the ability to resolve the chemical variations associated within fine scale histological features in extant and fossil bone.[8–13] Here we present the first histological and trace element analyses of bones from extinct cave hyaena (*Crocuta crocuta spelaea*) and extant spotted hyaena (*Crocuta crocuta*) to determine (1) whether cyclic growth can be correlated with differential distributions of trace elements crucial for bone growth and (2) if these elements can be preserved in fossilised tissues. Hyaenas were chosen based on the identification of zonal bone in other Pleistocene mammals and in extant arctic carnivores, both of which experience extremely high seasonal stress.[1,2,5] Cave hyaena are also very closely related to extant hyaena species (subspecies of spotted hyaena), thus limiting the amount of change in physiology due to taxonomic separation distance.

Methods

Specimens

Specimens consisted of four extant spotted hyaena (*C. crocuta*; ribs; Fig. S1†) consisting of both male (AMNH 87769, 83593) and female (AMNH 114226, 114227) specimens, and three extinct cave hyaena (*C. c. spelaea*; radius LL.20879, metacarpal LL.2200 and limb bone fragment P.3062; Fig. S2†). All extant specimens are from the American Museum of Natural History, New York, NY. The fossil specimen (P.3062) is from the Manchester Museum, Manchester, UK. Unfortunately, the same set of skeletal elements could not be sampled for both extant and fossil specimens due to the fragmentary nature of the fossil samples and the restrictions on destructive sampling of limb bones from extant material. Samples of bone from extant hyaena represent individuals that had been wild caught as captive animals are less likely to develop zonal tissue due to conditions provided in captivity (ex. zoo). Fossil material was obtained from the Pin Hole (radius LL.20879 and metacarpal LL.2200; 37.8 ka) and Church Hole Caves (indent. fragment P.3062; 26.84 to 24 ka), Creswell Crags, UK (Fig. S3†).[16] Due to the fragmented nature of the limb bone,

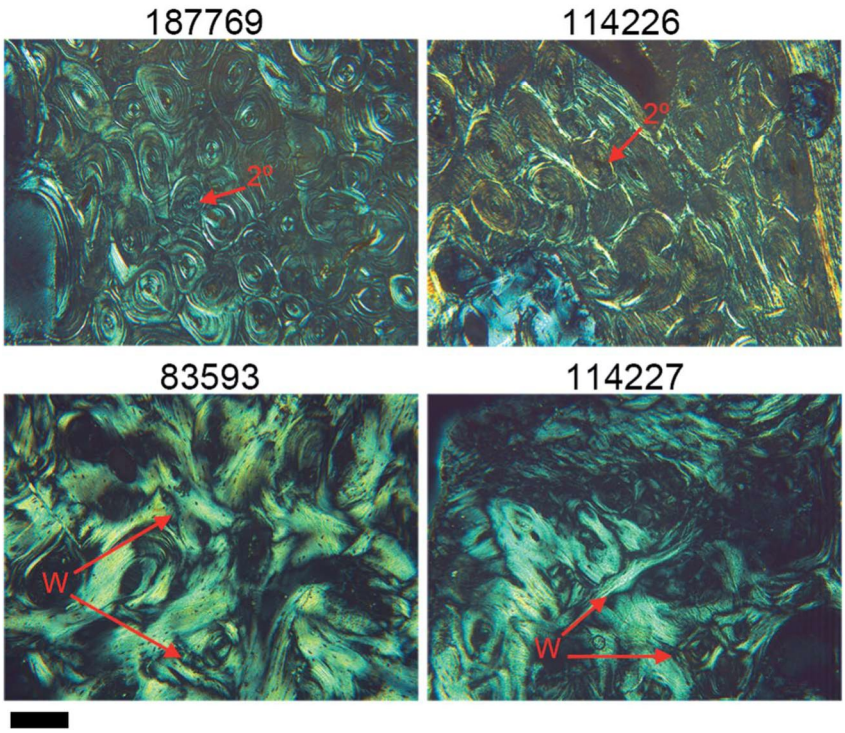

Fig. 1 Optical histology of extant hyena. Optical histology under cross-polarized light of *C. crocuta* ribs in adult male (AMNH 187769, 83593) and female (AMNH 114226, 114227) specimens. All specimens can be divided into two tissue types: highly remodelled with secondary osteons ('2°') or woven tissues ('W'). Scale bar is 200 μm.

faunal identification was confirmed using collagen fingerprinting (Fig. S4†).[17]

Optical histology

Thin sections were cut to a final thickness of ~25–50 μm. Sections were viewed using a Nikon ECLIPSE E600 POL microscope and ACT-1 software and a Leica DM2700P microscope and Leica Application Suite software under plain polarized and cross polarized light at 2×, 4×, and 10× magnifications. The billet or 'thick section' left from the thin section was used for chemical analyses, with no further sample preparation performed.

Synchrotron analyses

Synchrotron Rapid Scanning X-Ray Fluorescence (SRS-XRF) was conducted at beamline 6-2 at the Stanford Synchrotron Radiation Lightsource (SSRL; CA, USA). Detailed descriptions of SRS-XRF mapping applied to fossils are provided in recent publications[9,18–23] and are summarised here. Maps were collected with an incident beam energy of either 13.5 keV (high-*Z*; Ca and higher) or 3.15 keV (low-*Z*; Ca and lower). Specimens were mounted on an *x*–*y*–*z* stage and rastered relative to the fixed incident beam, with a 50 μm (fossil specimen) or 25 μm (extant specimens) beam diameter. Areas of interest in the fossil hyaena identified by SRS-XRF mapping were then mapped at higher spatial resolution at the Diamond Light Source (DLS; Oxfordshire, UK), beamline I-18, using the experimental setup of.[8,9,19] Maps were made using 5.5 μm beam diameter produced *via* Kirkpatrick–Baez focusing mirrors, with incident beam energy of 17 keV (chosen to allow excitation of the Sr Kα emission). X-ray flux was 10^{10}–10^{11} photons per s ('microfocus').

Single location energy dispersive spectra (EDS) were taken at both synchrotrons to quantify elements in discrete features (identified on elemental maps) by collecting a full EDS for 50 s (SSRL) or 30 s (DLS). Multiple spectra were taken per area of interest to account for heterogeneity within the sample. Spectra were fitted using PyMCA software (ex. Fig. S5†).[24] A Durango apatite mineral standard of known element concentrations was used for calibration.

Zinc Extended X-ray Absorption Fine Structure spectroscopy (EXAFS) was performed at DLS beamline I-18 to k space = 12. The Zn K-edge was calibrated using a Zn-foil. Background

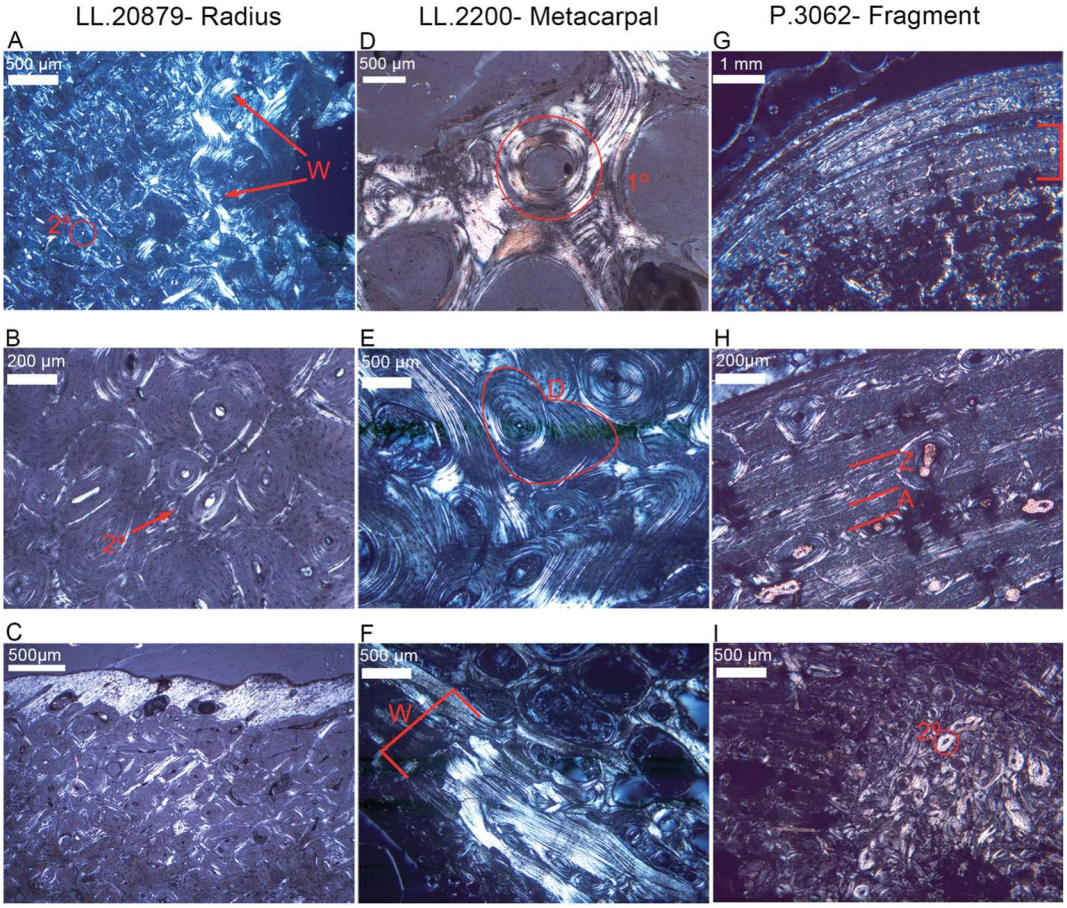

Fig. 2 Optical histology for cave hyena. Optical histology of the extinct cave hyaena, *C. c. spelaea*, radius (LL.20879; A–C), metacarpal (LL.2200; D–F) and limb fragment (P.3062; G–I) under cross polarized light. The radius consists of areas of secondary osteons ('2°'; A and B) and woven bone ('W'; A). In some regions, the periosteal surface has a fabric that is oriented obliquely to the more remodelled internal bone tissue (C). The metatarsus consists of dense primary osteons ('1°'; D) and drifting osteons ('D': E) interspersed with woven bone ('W'; F). Zonal bone is recognized in the limb fragment (G and H) with zones characterised by high porosity, with elongated osteons ('Z'; H) and annuali characterised by densely compact lamellar bone between annuali ('A'; H). A mass of secondary osteons is present, crossing perpendicular to the zones ('2°'; I).

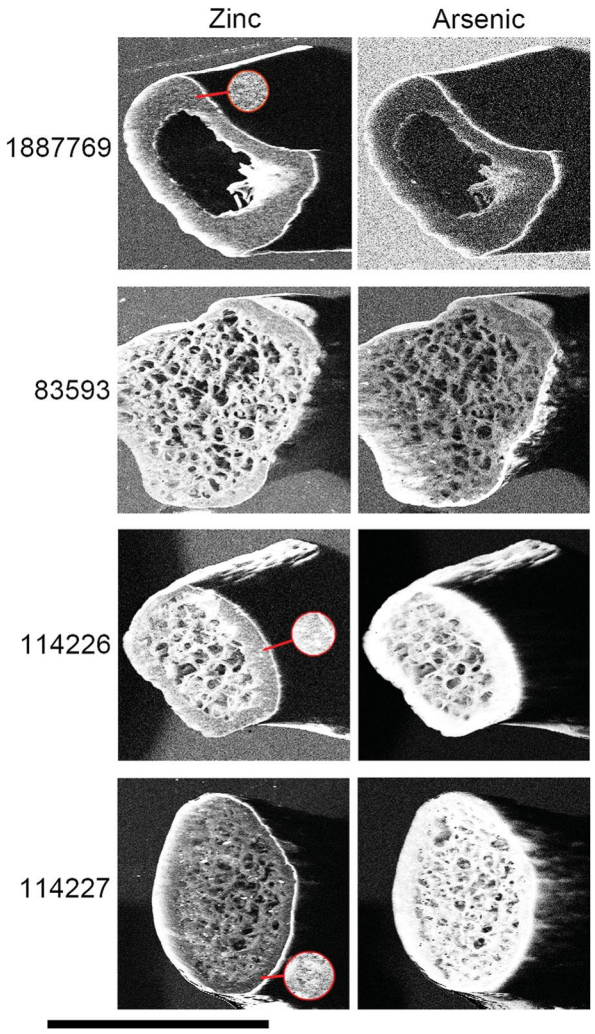

Fig. 3 Elemental maps of extant hyaena. Optical large-scale (centimetre) elemental maps of Zn and As in *C. crocuta* ribs (extant: male AMNH 87769, 83593; female AMNH 114226, 114227; fossil: P.3062). Bright areas represent relatively higher concentrations (photon counts). The counts in each elemental map are converted to 8 bit tiff images (scaled from 0 to 255) and thus is independently scaled and does not represent relative intensities compared to another elemental map. In Zn, higher concentrations (white) are associated with remodelling in secondary osteons (arrow and inset). Concentrations of As are elevated in the two female samples (AMNH 114226, 114227), but is uniformly distributed throughout the bone cross section. Scale bar is 1 cm.

subtraction, data normalization and fitting were performed using (d) Athena and (d) Artemis.[25] Spectra were compared to extant mammal bone and Zn-Hydroxyapatite (HAP) references.[26]

Results

Optical histology

Optical histology of the extant *C. crocuta* ribs shows a combination of densely packed secondary osteons ('2°'; Fig. 1) and areas of woven tissue running through the specimen into the cancellous struts ('W'; Fig. 1). No apparent differences between male (AMNH 187769 and 83593) and female (AMNH 114226 and 114227) specimens were observed.

Optical histology of the extinct *C. c. spelaea* radius and metacarpal (LL.20879 and LL.2200) revealed similar histological patterns as the extant material, with a mixture of woven bone ('W'; Fig. 2A and F) and secondary osteons ('2°'; Fig. 2A and B). Additional histological features include primary ('1°'; Fig. 2D) and drifting ('D'; Fig. 2E) osteons (osteon running both longitudinally and transversely through cortex). The radius also shows fabric that is oriented obliquely to the more remodelled internal bone tissue situated around the outer cortex (Fig. 2C). The fossil limb bone fragment (P.3062) shows zonal bone growth, seen as alternating bands of fast-growth (zones) and slow-growth (annuli) fibrolamellar tissues (brackets; Fig. 2G and H). Zones are identified by elongated osteons with large canal openings aligned in a 'ring' following the circumference of the bone section ('Z'; Fig. 2H). Annuli are identified by tightly packed lamellar bone forming another 'ring' ('A'; Fig. 2H). Thus, zones are identified as areas of bone tissue that are significantly more vascularised than annuli. A series of secondary osteons is seen in two isolated locations, with the osteons overprinting the original cortex through the entire cortical thickness ('2°'; Fig. 2I).

SR-XRF

XRF large-scale mapping (decimetre scale) shows Zn to be concentrated within secondary osteons (arrow and inset; Fig. 3). Differences in the elemental inventories between male and female are seen in Ca, Mn and As, with higher concentrations seen in female specimens (Fig. 3; Tables 1 and S1†). No other elements could be correlated with specific histological features or tissue types.

Table 1 Synchrotron XRF quantification of trace elements taken at SSRL (extant *C. crocuta*) and DLS (extinct *C. c. spelaea*; P.3062) given in ppm or weight percent (%). Extant *C. crocuta* measurements represent an average over the cortical bone as no zonal tissues were present. Fit errors are given in parentheses and represent ± two standard deviations

		C. crocuta (avg)		*C. c. spelaea* fragment	
	Mineral standard	Male	Female	Annuli	Zone
Ca	38.38% (2.27%)	32.19% (2.06%)	36.42% (2.26%)	23.47% (0.81%)	25.13% (0.78%)
Mn	—	2 (0.4)	133 (26)	56 (8)	145 (16)
Fe	902 (30)	37 (4)	51 (8)	136 (17)	175 (20)
Cu	—	5 (1)	3 (1)	1 (0.2)	3 (0.5)
Zn	77 (3)	130 (9)	134 (10)	165 (16)	384 (31)
As	2185 (68)	11 (1)	389 (21)	9 (1)	3 (0.4)
Sr	1885 (47)	—	—	421 (23)	405 (20)

Large-scale (centimetre) and microfocus elemental maps of the extinct *C. c. spelaea* limb bone fragment (P.3062) are presented in Fig. 4. Elemental maps of Zn revealed a pattern of relative high and low Zn banding (arrow; Fig. 4C). These bands were shown to correlate with the cyclic bands of zones and annuli, with higher concentrations in zones ('Z'; Fig. 4D). As in extant hyaena, Zn was also found to be associated with secondary osteons (circle; Fig. 4D). Arsenic is elevated within the medullary cavity and a section of the cortical bone not associated with the zones (Fig. 4E), and is present within the

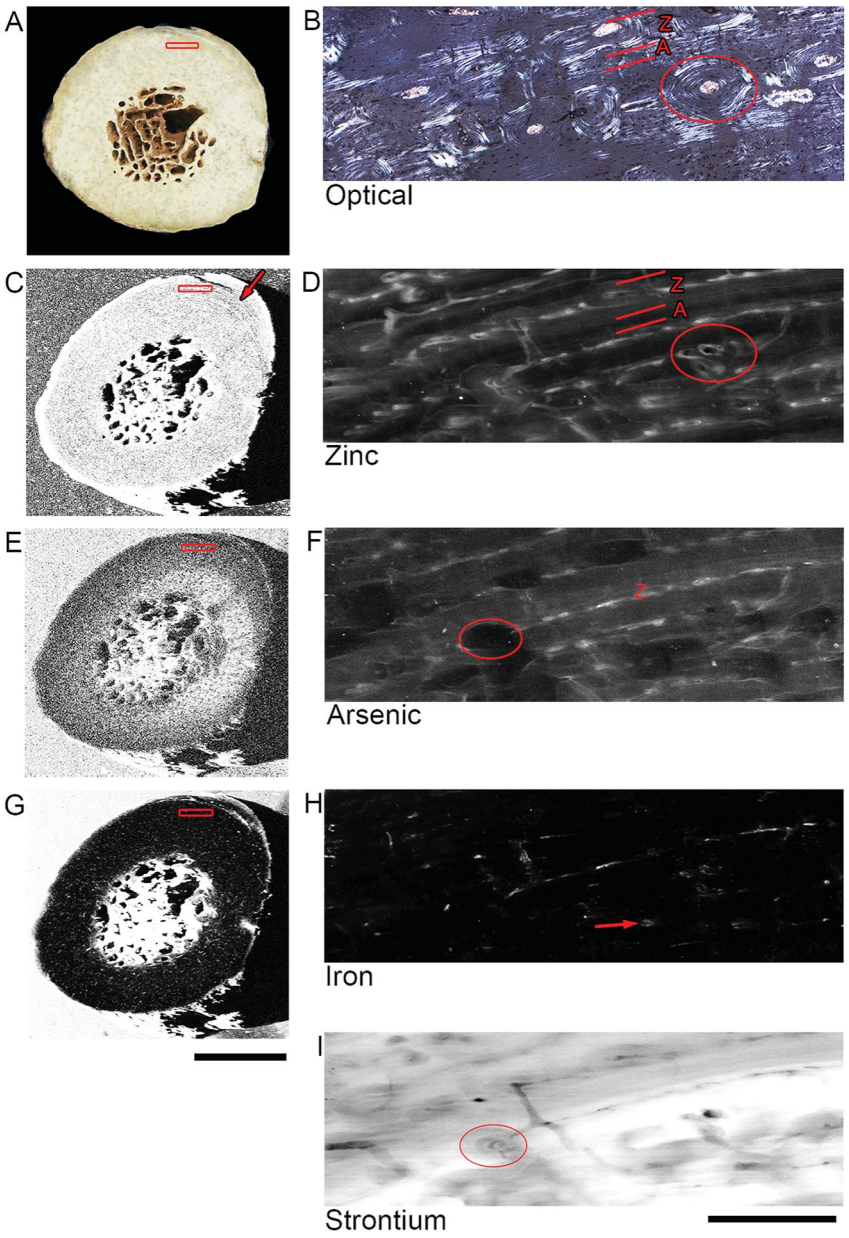

Fig. 4 Elemental maps of cave hyena specimen P.3062. Optical large-scale (centimetre) and histological images (A, B) of *C. c. spelaea* limb fragment (P.3062) compared to large and fine scale elemental maps of Zn (C, D), As (E, F), Fe (G, H) and Sr (I). Boxes on the large-scale images represent areas of interest highlighted in microfocus. Large-scale elemental maps of Sr are unavailable due to not being able to achieve the excitation energy for Sr on beamline 6-2 at SSRL. Bright areas represent relatively higher concentrations (photon counts). The counts in each elemental map are converted to 8 bit tiff images (scaled from 0 to 255) and thus is independently scaled and does not represent relative intensities compared to another elemental map. Large-scale elemental mapping shows regular banding of high/low Zn (arrow; C). Microfocus mapping shows these bands are correlated to the differences in zonal tissue, with higher Zn concentration correlated to zones ('Z'; D). Higher concentrations of Zn are also seen in association with secondary osteons (circle; D). In the large image, As is seen to be concentrated within the medullary cavity and a section of the cortical bone not associated with the Zn banding (E). However, in microfocus imaging bands of As do correlate to the differences in zonal tissue, with higher concentration correlated to zones ('Z'; F). Arsenic is also anti-correlated with secondary osteons (circle; F). Fe is mainly concentrated within the medullary cavity (G) and the mineral infill within osteon canals (arrow; H). Sr is slightly depleted within secondary osteons, with the exception of elevated 'rings' seen in the osteon highlighted (circle; I). Scale bar is 1 cm for large-scale images and 1 mm for microfocus.

Table 2 Fit statistics for Zn EXAFS in extant bone and P.3062 using (d) Artemis (5) and HAP with 412 ppm Zn taken from.[26] Errors are given as (±) the last significant figure unless specified. Error for CN is 25%. CN—coordination number; R(Å)—atomic distance (Å); σ^2 (Å^2)—Debye–Waller factor; ΔE_0 (eV)—shift in energy from calculated Fermi level; S0^2—amplitude factor; R—goodness of fit

Specimen	Path	CN	R (Å)	σ^2 (Å^2)	ΔE_0 (eV)	S0^2	χ^2	R
Extant	Zn–O	4.4	1.95(07)	0.007(1)	1.95 ± 0.77	0.99(3)	92	0.01
Fossil	Zn–O	4.2	1.95(05)	0.007(0.09)	2.14 ± 0.56	1.00(2)	17.26	0.007
Zn HAP (412 ppm)[26]	Zn–O	4.4	1.96	0.005	−0.53	—	—	0.073

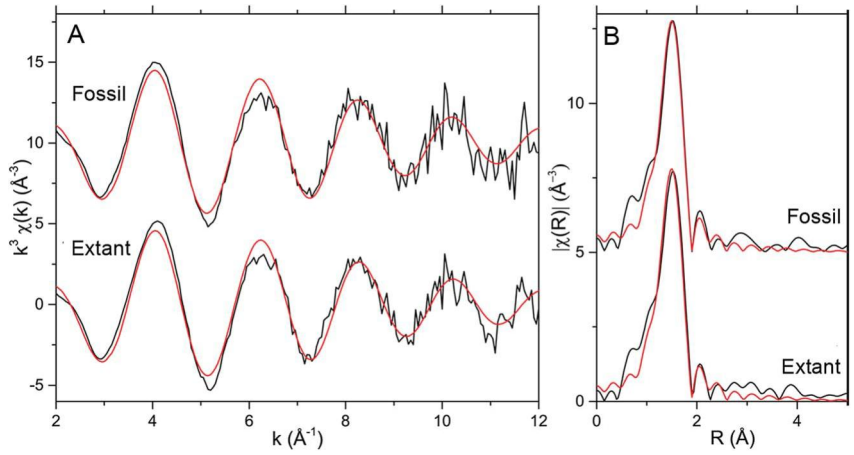

Fig. 5 Zinc EXAFS. Comparison of the Zn EXAFS spectra from the fossil and extant bone in k (A) and R-space (B) show Zn coordination is identical in the fossil and extant bone tissues.

primary bone tissue, but not within secondary osteons (Fig. 4F; circle). Fe is elevated within the medullary cavity (Fig. 4G) and areas of mineral infill (Fig. 4H; arrows). Sr is slightly elevated within the cement rings of the osteon (Fig. 4I; circle).

Trace element concentrations from the fossil limb bone fragment (P.3062) are within the range known for extant material,[8–10,27] with slight depletion in Ca and enrichment in Fe and Sr (Table 1). Elevated areas of Zn are approximately double the concentration of "low" Zn areas. Concentrations from non-elevated areas are comparable to cortical bone concentrations from extant material scanned in this study (Table 1).

Spectroscopy

X-ray absorption spectroscopy was performed to determine the coordination chemistry Zn within the bones in order to investigate whether the Zn could be derived from the original biochemistry of the organisms or if it had been replaced through taphonomic processes. Zn EXAFS of P.3062 revealed a tetrahedral coordination with four-O atoms at a distance of 1.95 Å (Table 2). This coordination and spacing is comparable to modern tissues (Fig. 5; Table 2), and Zn-HAP with concentrations of Zn comparable to modern bone (200–400 ppm), suggesting Zn was precipitated into the tissue during growth and is not surface contamination.

Discussion

The combination of optical and chemical histological analyses revealed Zn to be correlated within the fast growth tissues (zones) of zonal bone within an extinct cave hyaena (*C. c. spelaea*) limb fragment (P.3062; Fig. 4C and D) and within areas of active remodelling in extant hyaena (*C. crocuta*; Fig. 2) and cave hyaena (Fig. 4C and D). This observation fits with previous studies showing that enhanced Zn concentrations can be found within areas of active ossification and bone growth,[8–11,13–15] and that Zn is stable within the apatite structure of bone for extended periods of geologic time.[8,9,12,27]

This study reports the first case of zonal tissue within the Hyaenidae, both extant and fossil. The series of alternating high and low vascularity is interpreted as zonal tissue based on the regular deposition over a large area of the external cortex, which suggests deposition over time. It is not possible to state that each pair of zones/annuli correlates to one year of growth as there are numerous potential physiological and environmental factors that could also result in this alternating deposition (as discussed in the introduction). Intraskeletal variation could be one of the reasons for the lack of zonal tissue seen in the other two fossil hyaena (radius and metatarsal). It is interesting to note that the fossil hyaena displaying cyclic growth is from a stadial (colder phase; ~25 ka) of the last ice age, whereas the specimens without annular zones are from an interstadial (warmer phase; ~38 ka).[28] Future work is needed to test the hypothesis of whether extreme seasonal differences may have caused the differences observed between individuals.

Concentrations of Zn follow the pattern of zones and annuli, with higher concentrations correlating to zones (high rates of bone deposition). The correlation between high Zn and increased bone deposition fits within previous observations

that Zn is important in areas of active growth such as around growth plates and within osteons.[8,10,13–15] Zn levels within the zones of the fossil limb fragment (P.3062) are higher than the average concentrations measured in extant hyaena in this study, but are within the range seen in other terrestrial carnivores and humans.[10,27] The elevated regions within the zones are thin, and therefore the average Zn concentration in the fossil bone will be closer to reported bulk Zn concentrations in unzoned bone. EXAFS spectroscopy shows that the Zn is positively associated with fossil bone tissue, most notably the fast-growth zonal tissues, strengthening the hypothesis that Zn is endogenous to the specimen (Fig. 5C and D).

Elemental mapping also revealed interesting distributions of As, Fe and Sr within the fossil limb bone fragment (P.3062). Arsenic is associated with zonal tissue, though it is completely absent within osteons (Fig. 4E and F). In extant specimens, it is difficult to discern the origins of As given concentrations of As in the extant bone samples are variable probably due to its occasional use as a preserving agent in museum collections. Therefore we should not attempt to compare concentrations of As between the extant and fossil specimens. Concentrations of Fe suggest some diagenetic input as Fe levels are slightly elevated compared to extant bone (Fe 10–50 ppm; Goodwin *et al.*, 2007; Table 1), but not as heavily elevated as those seen in archaeological/fossil specimens (Fe 500–60 000 ppm).[29,30] Sr distributions show lower concentrations of Sr within secondary osteons compared to the surrounding tissue, with the exception of the cement lines that form as the osteon is filled in by separate layers of lamellar bone (Fig. 4I). Concentrations of Sr are between expected levels for extant terrestrial carnivores[27] and recent archaeological samples (less than 1000 years old)[11,29] suggesting little to no diagenetic input.

Conclusion

Correlation between histological features and chemical inventories strengthen the link between morphology and physiological processes, generating a *de novo* approach to the study of extinct organismal physiology. In this study, cyclic growth was correlated with differential distribution of Zn between fast (zones) and slow (annuli) growing bone tissue in the limb fragment of an extinct cave hyaena, *C. c. spelaea* (P.3062). The ability to resolve the subtle difference in biological chemistry between bone tissue types was only possible using the multi-scale mapping capabilities of synchrotron analyses. These results highlight the implications of using trace-element markers as a means for improving the analysis of archaeological and fossil bone.

Author contributions

All authors contributed in the synchrotron analysis and commented on the manuscript. JA, RAW and PLM designed the experiment. JA performed the optical histological analysis, processed the synchrotron data, wrote the manuscript and composed the figures. AvV processed and fit the EXAFS data, and composed Fig. 5 and Table 2. MB conducted the proteomics analyses (ESI†).

Funding

All authors acknowledge financial support from NERC (NE/J023426/1), the Royal Society (UF120473), the Jurassic Foundation (awarded JA), and the University of Manchester Dean's Award Fund (awarded JA). PLM thanks the Science and Technology Facilities Council for their support (ST/M001814/1).

Conflicts of interest

There are no conflicts to declare.

Acknowledgements

We thank the facilities and support staff of the Stanford Synchrotron Radiation Lightsource (3959) and Diamond Light Source (SP9488). Use of the Stanford Synchrotron Radiation Lightsource, SLAC National Accelerator Laboratory, is supported by the U.S. Department of Energy, Office of Science, Office of Basic Energy Sciences under Contract No. DE-AC02-76SF00515. The SSRL Structural Molecular Biology Program is supported by the DOE Office of Biological and Environmental Research, and by the National Institutes of Health, National Institute of General Medical Sciences (including P41GM103393). The contents of this publication are solely the responsibility of the authors and do not necessarily represent the official views of NIGMS or NIH. We thank the Manchester Museum (U.K), Academy of Natural Sciences of Drexel University (USA) and the American Museum of Natural History (USA) for access to specimens. Lastly, we thank Professor Andrew Chamberlain for his invaluable advice.

References

1 M. Köhler, N. Marin-Moratalla, X. Jordana and R. Aanes, Seasonal bone growth and physiology in endotherms shed light on dinosaur physiology, *Nature*, 2012, **487**, 358–361, DOI: 10.1038/nature11264.

2 A. Chinsamy-Turan, *Forerunners of Mammals: Radiation Histology Biology (Life of the Past)*, Bloomington, Indiana University Press, 2011.

3 M. Köhler and S. Moyà-Solà, Physiological and life history strategies of a fossil large mammal in a resource-limited environment, *Proc. Natl. Acad. Sci. U. S. A.*, 2009, **106**(48), 20354–20358.

4 J. Castanet, Time recording in bone microstructures of endothermic animals; functional relationships, *Comptes Rendus Palevol*, 2006, **5**, 629–636.

5 A. Chinsamy-Turan, *The Microstructure of Dinosaur Bone: Deciphering Biology with Fine-scale Techniques*, Baltimore, The Johns Hopkins University Press, 2005.

6 A. Chinsamy and P. Dodson, Inside a dinosaur bone, *Am. Sci.*, 1995, **83**, 174–180.

7 C. Kolb, T. M. Scheyer, K. Veitschegger, A. M. Forasiepi, E. Amson, A. A. E. Van der Geer, *et al.*, Mammalian bone palaeohistology: a survey and new data with emphasis on island forms, *PeerJ*, 2015, **3**, e1358.

8 J. Anné, R. A. Wogelius, N. P. Edwards, A. van Veelen, K. Ignatyev and P. L. Manning, Chemistry of bone remodelling preserved in extant and fossil Sirenia, *Metallomics*, 2016, **8**(5), 508–513, DOI: 10.1039/c5mt00311c.

9 J. Anné, N. P. Edwards, R. A. Wogelius, A. R. Tumarkin-Deratzian, W. I. Seller, A. van Veelen, *et al.*, Synchrotron imaging reveals bone healing and remodelling strategies in extinct and extant vertebrates, *J. R. Soc., Interface*, 2014, **11**(96), 20140277.

10 B. Pemmer, A. Roschger, A. Wastl, J. G. Hofstaetter, P. Wobrauschek, R. Simon, *et al.*, Spatial distribution of the trace elements zinc, strontium, and lead in human bone tissue, *Bone*, 2013, **57**, 184–193.

11 T. Swanston, T. Varney, I. Coulthard, R. Feng, B. Bewer, R. Murphy, *et al.*, Element localization in archaeological bone using synchrotron radiation x-ray fluorescence: Identification of biogenic uptake, *J. Archaeol. Sci.*, 2012, **39**(7), 2409–2413, DOI: 10.1016/j.jas.2012.01.041.

12 A. Kuczumow, E. Cukrowska, A. Stachniuk, R. Gawęda, R. Mroczka, W. Paszkowicz, *et al.*, Investigation of chemical changes in bone material from South African fossil hominid deposits, *J. Archaeol. Sci.*, 2010, **37**, 107–115.

13 C. O. Molokwu and Y. V. Li, Zinc homeostasis and bone mineral density, *Ohio Res. Clin. Rev.*, 2006, **15**, 7–15.

14 G. L. Hammond, G. V. Avvakumov and Y. A. Muller, Structure/function analyses of human sex hormone-binding globulin: effects of zinc on steroid-binding specificity, *J. Steroid Biochem. Mol. Biol.*, 2003, **85**(2–5), 195–200, DOI: 10.1016/S0960-0760(03)00195-X.

15 S. Gomez, R. Rizzo, M. Pozzi-Mucelli, E. Bonucci and F. Vittur, Zinc mapping in bone tissues by histochemistry and synchrotron radiation-induced X-ray emission: correlation with the distribution of alkaline phosphates, *Bone*, 1999, **25**(1), 33–38.

16 R. E. M. Hedges, P. B. Pettitt, C. B. Ramsey and G. J. van Klinken, Radiocarbon dates from the Oxford AMS system: Archaeometry datelist 22, *Archaeometry*, 1996, **38**(2), 391–415.

17 L. G. van der Sluis, H. I. Hollund, M. Buckley, P. G. B. De Louwd, K. F. Rijsdijke and H. Kars, Combining histology, stable isotope analysis and ZooMS collagen fingerprinting to investigate the taphonomic history and dietary behaviour of extinct giant tortoises from the Mare aux Songes deposit on Mauritius, *Palaeogeogr., Palaeoclimatol., Palaeoecol.*, 2014, **416**, 80–91.

18 V. Egerton, R. A. Wogelius, M. A. Norell, N. P. Edwards, W. I. Sellers, U. Bergmann, *et al.*, The mapping and differentiation of biological and environmental elemental signatures in the fossil remains of a 50 million year old bird, *J. Anal. At. Spectrom.*, 2015, **30**, 627–634, DOI: 10.1039/c4ja00395k.

19 N. P. Edwards, P. L. Manning, U. Bergmann, P. L. Larson, B. E. van Dongen, W. I. Sellers, *et al.*, Leaf metallome preserved over 50 million years, *Metallomics*, 2014, **6**(4), 774–782.

20 P. L. Manning, N. P. Edwards, R. A. Wogelius, U. Bergmann, H. E. Barden, P. Larson, *et al.*, Synchrotron-based chemical imaging reveals plumage patterns in a 150 million year old early bird, *J. Anal. At. Spectrom.*, 2013, **28**(7), 1024–1030, DOI: 10.1039/c3ja50077b.

21 N. P. Edwards, R. A. Wogelius, U. Bergmann, P. Larson, W. I. Sellers and P. L. Manning, Mapping prehistoric ghosts in the synchrotron, *Appl. Phys. A: Mater. Sci. Process.*, 2013, **111**(1), 147–155, DOI: 10.1007/s00339-012-7484-3.

22 R. A. Wogelius, P. L. Manning, H. E. Barden, N. P. Edwards, S. M. Webb, W. I. Sellers, *et al.*, Trace metals as biomarkers for eumelanin pigment in the fossil record, *Science*, 2011, **333**(6049), 1622–1626, DOI: 10.1126/science.1205748.

23 U. Bergmann, R. W. Morton, P. L. Manning, W. I. Sellers, S. Farrar, K. G. Huntley, *et al.*, Archaeopteryx feathers and bone chemistry fully revealed *via* synchrotron imaging, *Proc. Natl. Acad. Sci. U. S. A.*, 2010, **107**(20), 9060–9065.

24 V. A. Solé, E. Papillon, M. Cotte, Ph. Walter and J. Susini, A multiplatform code for the analysis of energy-dispersive X-ray fluorescence spectra, *Spectrochim. Acta, Part B*, 2007, **62**(1), 63–68, DOI: 10.1016/j.sab.2006.12.002.

25 B. Ravel, M. A. Newville and H. Artemis, Data Analysis for X-ray Absorption Spectroscopy using IFEFFIT, *J. Synchrotron Radiat.*, 2005, **12**, 537–541, DOI: 10.1107/s0909049505012719.

26 Y. Tang, H. F. Chappell, M. T. Dove, R. J. Reeder and Y. J. Lee, Zinc incorporation into hydroxylapatite, *Biomaterials*, 2009, **30**(15), 2864–2872.

27 J. C. Sealy and A. Sillen, Sr and Sr/Ca in marine and terrestrial foodwebs in the southwestern cape, South Africa, *J. Archaeol. Sci.*, 1988, **15**, 425–438.

28 S. O. Rasmussen, M. Bigler, S. P. Blockley, T. Blunier, S. L. Buchardt, H. B. Clausenet, *et al.*, A stratigraphic framework for abrupt climatic changes during the Last Glacial period based on three synchronized Greenland ice-core records: refining and extending the INTIMATE even stratigraphy, *Quat. Sci. Rev.*, 2014, **106**, 14–28.

29 M. L. Carvalho, A. F. Marques, M. T. Lima and U. Reus, Trace elements distribution and post-mortem intake in human bones from middle age by total reflection X-ray fluorescence, *Spectrochim. Acta, Part B*, 2004, **59**(8), 1251–1257.

30 M. B. Goodwin, P. G. Grant, G. Bench and P. A. Holroyd, Elemental composition and diagenetic alteration of dinosaur bone: distinguishing micron-scale spatial and composition heterogeneity using PIXE, *Palaeogeogr., Palaeoclimatol., Palaeoecol.*, 2007, **253**, 358–476.